MFN= 007177
01 SID/SCD
02 5767
03 INPE-5767-PRE/1928
04 CEA
05 S
06 as
10 Aguiar, Odylio Denys
10 Johnson, W.W.
10 Hamilton, W.O
12 A cryogenic double-resonant parabridge motion transducer for resonant-mass gravitational wave detectors
14 2523-2534
30 Review of Scientific Instruments
31 62
32 11
40 En
41 En
42 <E>
58 DAS
61 <PI>
64 Nov. <1991>
68 PRE
76 ASTROFISICA
83 We designed, constructed and tested at 4.2 K (using two different low phase noise electrical pump generators) a cryogenic double-resonant parabridge motion transducer made out of niobium, whose electrical output was amplified by a two-stage metal-semiconductor field-effect transistor cryogenic amplifier. Most of the experimental results agreed well with the theoretical models. We were able to adjust the two electrical bridge resonant frequencies at the pump frequency, allowing us to obtain an electromechanical coupling as high as 0.054, and we successfully measured the mechanical Brownian motion of this transducer. In one case, we observed a dip in the electrical noise spectrum near the mechanical resonant frequency due to destructive interference between this noise and its "reflection" from the mechanical resonator. At the bottom of this dip, in a bandwidth of 0.7 Hz, we measured an equivalent displacement noise of 4 x 10-16 m/ Hz with a systematic error of less than (10.%
88 DETECTORS
88 CRYOGENICS
90 b
91 FDB-19960325
92 FDB-MLR

A cryogenic double-resonant parabridge motion transducer for resonant-mass gravitational wave detectors

O. D. Aguiar,[a] W. W. Johnson, and W. O. Hamilton
Department of Physics and Astronomy, Experimental Gravitation Group, Louisiana State University, Baton Rouge, Louisiana 70803

(Received 26 November 1990; accepted for publication 8 July 1991)

We designed, constructed, and tested at 4.2 K (using two different low phase noise electrical pump generators) a cryogenic double-resonant parabridge motion transducer made out of niobium, whose electrical output was amplified by a two-stage metal-semiconductor field-effect transistor cryogenic amplifier. Most of the experimental results agreed well with the theoretical models. We were able to adjust the two electrical bridge resonant frequencies at the pump frequency, allowing us to obtain an electromechanical coupling as high as 0.054, and we successfully measured the mechanical Brownian motion of this transducer. In one case, we observed a dip in the electrical noise spectrum near the mechanical resonant frequency due to destructive interference between this noise and its "reflection" from the mechanical resonator. At the bottom of this dip, in a bandwidth of 0.7 Hz, we measured an equivalent displacement noise of 4×10^{-16} m/$\sqrt{\text{Hz}}$ with a systematic error of less than 10%.

I. INTRODUCTION

Most cryogenic resonant-mass gravitational wave detectors (or "telesensors"[1]) are composed of four major parts: (1) a massive bar which is resonant near 1 kHz, (2) a small-mass mechanical resonator tuned to the same frequency, (3) an electromechanical transducer, and (4) an electronic amplification chain. The solid bar, also called an "antenna," has a fundamental longitudinal mechanical resonance that can be excited by the passage of ripples in the spacetime curvature, or Einstein's gravitational waves.[2] The small-mass resonator is a tuned mechanical transformer, transforming small motions of the large mass bar into larger motions of the small-mass resonator. The electromechanical transducer transforms these mechanical motions into electrical signals which are then amplified by the electronic chain. The second and third major parts of the detector are so strongly coupled that they are often considered as a unit that is loosely called the "transducer."

Since the first bar detector model invented by Weber during the sixties, experimentalists have improved gravitational wave burst sensitivities by five orders of magnitude.[3] Even though there is some chance of detecting gravitational waves coming from the cosmos at this sensitivity,[4] reasonable estimates suggest we need to improve another five orders of magnitude to detect one event per month or so. A third generation of resonant-mass gravitational wave detectors are being built to accomplish this task.[5] This effort requires the construction of much better motion transducers, and a promising design relies on active transducer models, also called parametric transducers. These transducers have the capability to perform "back action evasion" and might surpass the standard quantum limit of a vibration amplitude measurement by carrying out a "quantum nondemolition measurement."[6] It is this kind of transducer that we have designed, built, and experimentally tested, the results of which are reported here.

Parametric transducers for use in gravitational wave detectors have been designed since the mid seventies.[7–11] The development of these transducers was intensified[12–15] after the first schemes of quantum nondemolition measurements were proposed.[16] These designs used either high-Q niobium cavities[17–20] or an electrical parabridge circuit with lead-coated sapphire capacitors.[21,22] The present design uses a niobium electrical parabridge circuit with a niobium capacitor as mechanical resonator; this capacitor is pumped at 5 MHz by an oscillator which had more than three orders of magnitude smaller phase noise than the oscillators used in previous designs. We also built a very effective vibration isolation system that gave us the capability to measure the mechanical resonator's Brownian motion for this transducer.

II. GENERAL DESIGN AND CONSTRUCTION

The electrical circuit for this parametric transducer is shown in Fig. 1. The middle plate of the three-plate capacitor is the mechanical resonator of this parametric transducer. The outer loop of the bridge is "pumped" at $f_p = 5$ MHz, and its resonance frequency f_{olr} is adjusted to a value as close as possible to f_p in order to enhance the pump signal across the capacitor plates. Impedance balancing guarantees a very small current in the middle branch for a motionless three-plate capacitor, to avoid saturating the amplifier chain with a signal at the pump frequency, and to minimize the presence of phase noise from the pump signal at the transducer output. In the presence of acceleration on the three-plate capacitor, the middle plate oscillates back and forth, changing both capacitances to the side plates. A current flows in the middle branch proportional to the middle plate displacement. This current is

[a]On leave from the Department of Astrophysics, Instituto Nacional de Pesquisas Espaciais (INPE), C.P. 515, 12201-São José dos Campos-SP, Brazil.

 0034-6748/91/112523-12$02.00

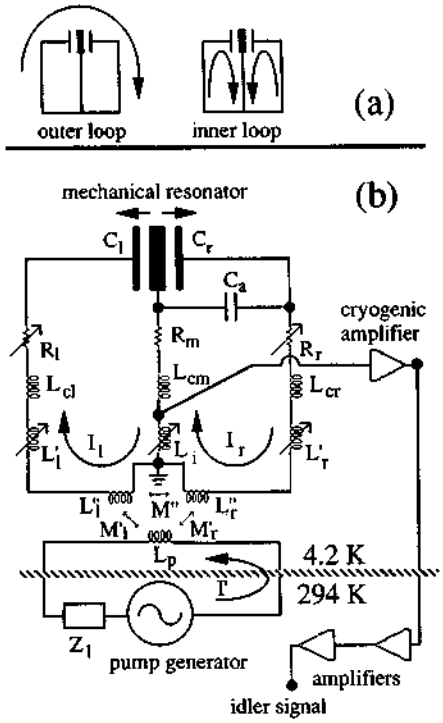

FIG. 1. The parabridge transducer electrical circuit. (a) A very simplified diagram showing the outer loop and inner loop currents, and (b) a more detailed schematic. The central plate of the three-plate capacitor is the mechanical resonator of this transducer. Balancing was achieved by adjusting the side inductances (L'_l and L'_r) and resistances (R_l and R_r). These inductances, together with the idler (readout) inductance (L_i), also could change the outer and inner loop resonant frequencies. We were able to vary the inductances by moving, with the help of motors, a niobium rod inside each of them. The resistive balancing was adjusted by controlling, with MESFET transistors, the resistances of two external loops coupled to each side branch. There was no capacitive adjustment. C_a is a fixed value additional capacitance to decrease the capacitive imbalance between C_l and C_r. L_{cl}, L_{cm}, and L_{cr} are cable inductances.

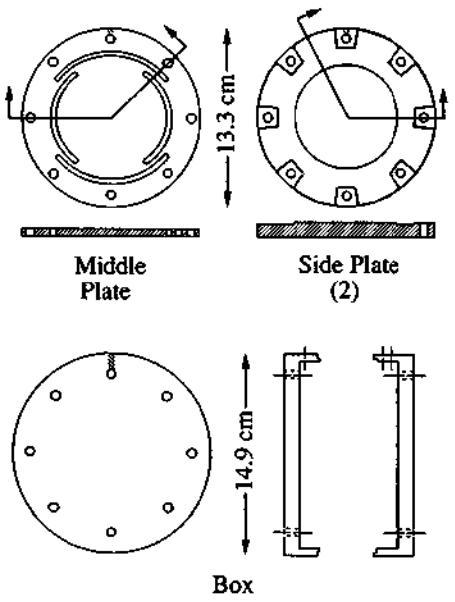

FIG. 2. Three-plate capacitor and shielding box. Due to the cuts in the middle plate, its central core was free to oscillate back and forth. The capacitances were formed by this central core and the circular "island" on each side plate. Mylar washers separated these three plates, and everything went inside a niobium shielding box. Eight titanium studs tightened the whole set to an aluminum flange.

proportional to the time derivative of the product between the voltage across the capacitor plates and its capacitance; therefore, it has two components (that we will call idler signals) at frequencies that are equal to the sum ($f_+ = f_p + f_m$) and difference ($f_- = f_p - f_m$) of the mechanical frequency and pump frequency. Each of these idler signals is enhanced if the inner loop resonant frequency f_{ilr} is such that $|f_{ilr} - f_\pm| < (f_{ilr}/Q_{ilr})$. The voltage generated across the idler (or readout) inductor by these currents is amplified by a two-stage metal-semiconductor field-effect transistor (MESFET) cryogenic preamplifier and a set of two amplifiers at room temperature. This voltage is demodulated and measured.

Figure 2 illustrates the three-plate capacitor plus shielding box. The middle plate has four built-in beams as springs. A gap of 50 μm was provided between the middle plate and each side plate by 16 mylar washers,[23] and a 1 mm gap between the side plates and the shielding box by another set of 16 1-mm-thick sapphire washers. The mylar washers as well as the sapphire washers are placed on the surface centered over each hole. A 1 mm depression was provided on the side plates just between the area where the mylar washers were placed and the central core in order to maximize the percentage of the capacitor that would act as transducer pickup. Eight titanium studs 6 mm in diameter fasten the "sandwich" assembly horizontally to an aluminum plate. These titanium studs were positioned to avoid electrical shorts between any plate and the shielding box to which the studs were grounded.

The mechanical pickup capacitor as well as all electrical components was made of high-purity niobium (>99.75%). The mechanical resonator was annealed to 925 °C at 2×10^{-7} Torr for 1 h. In order to minimize microphonics, the Nb wire used for making the inductors, the coaxial cables' inner conductors, and the general wiring had a diameter of 0.8 mm. Because of very low dielectric loss tangent,[24] teflon was used for the inductor's cases, transformer mounting, and coaxial dielectric. The entire niobium circuit was protected from external electrical noise by high-purity niobium shielding.

Figure 3 demonstrates the schematic setup of the experiment. The experimental can is 60 cm long and 30 cm in diameter. The aluminum flange, to which the transducer box is bolted, is both a vibration isolation stage and part of the calibration capacitor. It is a single piece made of 5056 aluminum alloy with two major sections: the core and the rim. The core has a base with eight holes and cavities for bolting the transducer. The top of the core has a circular 7-cm-diam flat island and a 3.2-cm-wide, 1.3-cm-deep annular depression around it. This core is connected to an outside rim by springs similar to those in the transducer middle plate, but much longer, and this rim is connected to the last stage of a vibration isolation stack by titanium wires 0.76 mm in diameter. The stiffness of these aluminum springs was designed,[25–27] so that if the rim was firmly

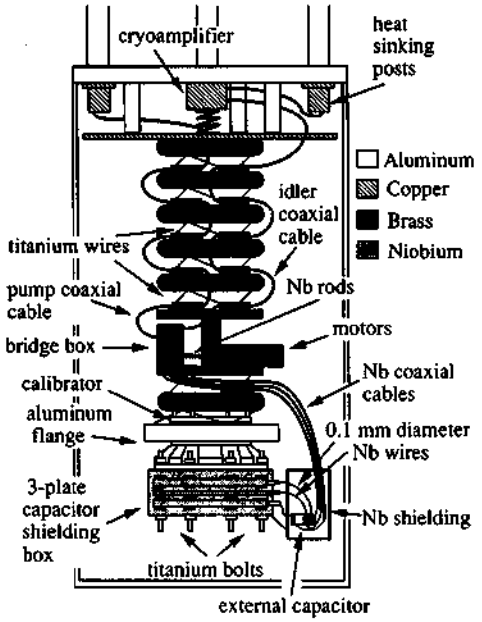

FIG. 3. Setup inside the cryostat's experimental space. This hollow cylindrical space of 30 cm in diameter and 60 cm in height, immersed in liquid helium, kept the parabridge and the vibration isolation system in vacuum. The latter, together with the air table, which suspended the whole cryostat, had an estimated attenuation of at least 14 orders of magnitude for vertical motions coming from the lab. The cryoamplifier was at the top for better thermal contact with the helium bath.

attached, the transducer box plus aluminum flange core (a total mass of 8.2 kg) would oscillate at a frequency of about 33 Hz. The circular island on the top of the aluminum flange faces a horizontal aluminum plate, similar to the transducer middle plate, which has its rim rigidly attached by a set of nylon bolts and nuts to the last stage of the vibration isolation stack. A distance of one-half inch is kept between the aluminum plate and the vibration isolation stage. The springs were machined in order to make this aluminum plate resonant in the 300 Hz vicinity, and, therefore, to be a free mass for the transducer. This capacitor was used to mechanically excite the transducer with a known signal. There was also a PZT sensor[28] glued to one of the flange's built-in springs. This PZT was used for noncalibrated excitations and as a vibration sensor during motor adjustment.

The bridge circuit is housed inside a niobium rectangular box which is attached to the second vibration isolation stage above the aluminum flange. This box is formed by six 4.7-mm-thick niobium rectangular plates 10.8 cm long and 5 cm wide. All six pieces are bolted together, forming a sandwich, by eight titanium bolts and five brass bolts.The internal cavities of the box were machined in its four central plates. The front plate has holes instead of cavities for insertion of 4.7-mm-diam niobium rods, and the rear plate has two tiny holes for outside connection between the circuit's middle branch and the transformer grounding point. An extra niobium grounding sheet covers the grounding connection on the rear. The transformer cavity is cubic, to house a toroidal transformer. All the other inductors are solenoids inside cylindrical cavities.

The transformer's secondary inside the bridge box was a toroidal coil made with a single 0.8-mm-diam Nb wire electrically insulated by teflon tubing. This wire was guided by a teflon block with one hole in the middle for the primary. The secondary was composed of 20 holes forming a circle of 0.53 cm radius and 20 holes forming another circle of 0.99 cm radius. The Nb wire used every other hole to do ten turns in the first rotation and another ten turns in the second rotation. This procedure guaranteed a very symmetrical transformer for both circuit branches and a good coupling coefficient between the two halves ($k = 0.56$). The grounding point was halfway between the end of one rotation and the beginning of the next one. First, this wire section went through a tiny hole in the box wall to meet one end of the idler inductor solenoid. There, both wires were plasma welded together,[29] and this welded joint was pressed against an Nb sheet grounded to the shielding box.

The idler inductor, as well as the right and left inductors, were solenoids housed inside teflon cases to keep them from springing out. Nb rods were free to move in and out of these solenoids. The mechanism used to transform the motor-gearbox rotation into a translational movement for the rods was very simple. A long brass hollow cylinder was firmly attached at one end to the gearbox axle. its other end had a 2-56 threaded hole in which a long steel 2-56 screw was inserted. Because this screw's rotation was impeded by a pin guided in a groove parallel to the screw, the only movement allowed was the translation along its axis. Each Nb rod was attached to one of these screws, so they followed the same movement. The typical rod speed for 10 mA of current running in one motor was about 1 mm/minute.

The MESFET transistors for resistance balancing were housed in the bridge box inside teflon pads. Two five-turn 275 nH copper coils were facing the end of each side inductor (right and left ones). Each of these coils was connected to the drain and source of one transistor. The voltage control between gate and drain was sent by two copper semi-rigid coaxial cables, one for each transistor. The transistors used for this purpose were Fujitsu FSC10FA, which presented a typical 23 Ω resistance between drain and source at 4.2 K for zero bias voltage.

The transition between the three-plate capacitor and the Nb coaxial cables circuit was formed by 0.1 mm Nb wires in order to mechanically decouple the three-plate capacitor from the external wiring as much as possible. Superconductive joints were made pressing these wires against other Nb parts after having cleaned them with an acid solution.[30] A 100 pF Nb capacitor was placed next to the three-plate capacitor. This extra capacitance was necessary to bring the two three-plate capacitances closer in absolute value. In the original design this capacitance was inside the bridge box, but it was abandoned in favor of the fixed-value capacitor placed next to the three-plate capacitor. This second design had the advantage of simplicity and reliability, but it could not balance the bridge at all frequencies. Because we were only able to adjust the bridge

inductively and resistively, a perfect balance could not be maintained at more than one frequency.

The cryogenic amplifier circuit design was inspired by a British version used in nuclear magnetic resonance (NMR) detection that presented a noise temperature of (1.3 ± 0.4) K below 77 K at 5 MHz.[31] The component values were changed to maximize power gain, to minimize noise, and to decrease power dissipation. The voltage gain was approximately 1 when cold, but the power gain for the 50 Ω input room-temperature amplifier was ~2000. The power dissipation was about 5 mW for 5.3 V bias voltage, as designed. The two FET transistors were GaAs Plessey P35-1101-101. We specifically used the characteristics of a similar device,[32] the P35-1101-1, to design this amplifier.[33]

The cryogenic amplifier shielding box was a hollow copper cylindrical box to which three soldered copper semi-rigid coaxial cables were connected. One brought the idler signal to the amplifier input, another sent the output to the top of the cryostat feedthrough, and the third was used for amplifier biasing. This copper box was pressed against the top of the experimental can by a strong spring for good thermal contact. A thermal grease, "Cry-con" from APD Cryogenics, was used for thermal contact enhancement. A paper on the top of the box and a teflon pad on the bottom prevented the box from being electrically grounded to the cryostat. The transducer grounding point was on the top of the cryostat, and only the idler coaxial cable was connecting this point to the transducer.

All the resistors used in the cryogenic amplifier were of metal film. The capacitors were silver mica, which maintained their values of capacitance at 5 MHz when cooled to 4.2 K. The circuit was soldered on a printed board with an extra ground plane. All ground regions were soldered to the copper shielding box. Both Plessey transistors were thermally grounded to this copper box with copper tape.

The vibration isolation system was composed of three parts. The first one consisted of an air table attached to the cryostat top plate supporting the whole experimental apparatus (~370 kg). This air table, model 71.401 manufactured by Lansing Research Corporation, caused displacements at frequencies f above $f_0 = 1.39$ Hz to decrease by the factor $= (f/f_0)^2$. The second part of this vibration isolation system was a set of cylindrical brass masses connected by titanium wires (6% Al-4% V-Ti alloy with a minimum yield strength of 84 kg/mm^2) and arranged in the form of a stack.[34] All the leads going down to the transducer were mechanically grounded to each of these stages. The wire diameter was chosen, in the present design, in order to have its first transverse string resonance above 1500 Hz. This choice would still keep the tension in each wire at least 1/3 of the yield. This vibration isolation stack, seen in Fig. 3, has seven stages. The third and last part of this vibration isolation system is the high-Q aluminum flange built-in springy arms with an attenuation factor equal to $(f/f_3)^2$ (where $f_3 = 33$ Hz and f is any frequency above this value). Theoretically, the vertical motions would be attenuated by 350 dB due to the presence of this vibration isolation system alone, but nonlinear effects and the electrical wiring attached to it should decrease its performance.

TABLE I. The most important physical parameters of the present parabridge transducer.

T	physical temperature	4.2	K
M	transducer's reduced mass	0.261	kg
m	resonator's mass	0.27	kg
f_m	mechanical resonant frequency	929.143	Hz
f_{ilr}	inner loop resonant frequency	4.9–5.2	MHz
f_{olr}	outer loop resonant frequency	4.9–4.98	MHz
Q_m	mechanical quality factor	138 k	
Q_{ilr}	inner loop resonance quality factor	2.2 k	
Q_{olr}	outer loop resonance quality factor	650	
D	capacitor gap	50	μm
C	capacitance	1.45	nF
L_0	total inner loop inductance	0.7	μH
L_i	idler (read-out) inductance	0.15	μH
VL_i/V_{cap}	imbalance (best measured)	12	ppm
β	coupling factor (highest meas.)	0.054	

III. EXPERIMENTAL TESTS

Table I shows a summary of the most important transducer parameters.

A. Parabridge tuning and balancing

We measured the voltage across the parabridge's idler inductor as a function of frequency for different conditions of tuning and balancing, and compared these results with the theoretical calculations derived from the equations of the electrical bridge circuit. Finally, we examined the theoretical conditions for bridge balance and tried to implement them in practice. Results were again compared with theory, and the residual capacitance imbalance and the noise leakage from the outer loop were determined.

The transducer circuitry has two electrical resonances: the outer and inner loop resonances. They were used to enhance the pump and idler signals, respectively. Figure 4 shows these two resonances and the equipment diagram to measure them. The higher frequency resonance in this figure, which is the inner loop resonance, had an electrical Q of about 2000. The motor adjustment of the idler inductor allowed us to tune the inner loop resonance between 4.9 and 5.1 MHz; unfortunately, we were not able to do the same with the outer loop resonance. The motor adjustment of the side inductors could balance the bridge, but not tune the outer loop resonance above 4.95 MHz, which prevented our fully pumping the capacitor when we were using the 5 MHz extremely low phase noise crystal oscillator. The fitting curve in Fig. 4 was calculated from the loop equations of the circuit shown in Fig. 1.

The transducer can achieve its best performance when the bridge is balanced. Balancing the bridge at the idler frequency impedes the noise generated in the outer loop at this frequency from entering the middle branch where the readout inductor is located. Furthermore, balancing the bridge at the pump frequency minimizes the idler inductor excitation at the pump (generator) frequency, because this excitation can saturate the amplification chain.

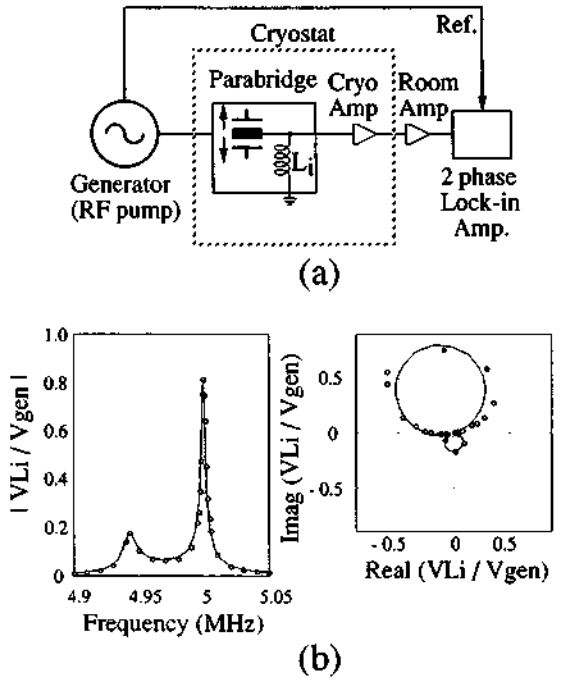

FIG. 4. Tuning and balancing the parabridge. (a) The schematic of the measurement setup, and (b) the response when the bridge was far from optimum tune and balance. The plotted quantity is the output voltage of the bridge, at the same frequency of the generator, normalized to the generator voltage. The circles are data and the line is the best fit to a solution of the loop equations and expected values for the electrical components. Notice the two resonance circles in the complex-plane plot.

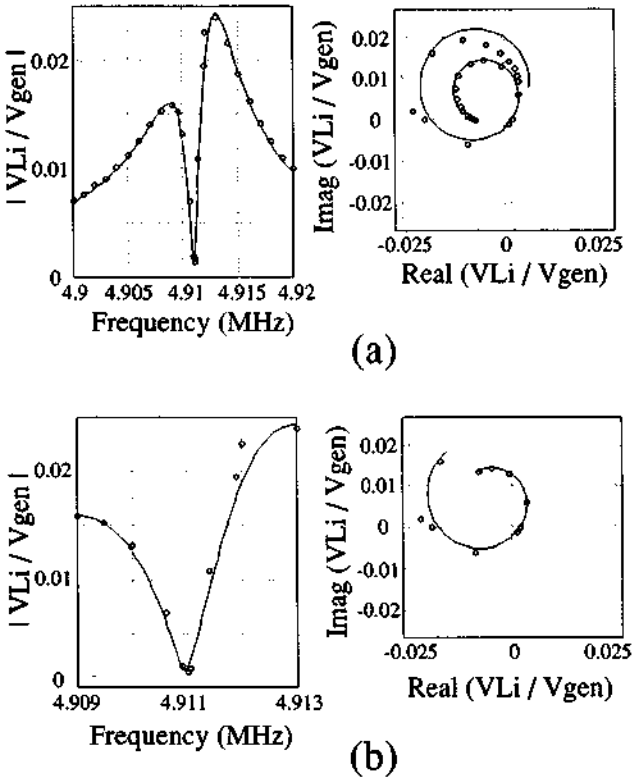

FIG. 5. (a) The response, for the arrangement of Fig. 4, when the bridge had good tune and balance. The inner loop resonance was moved to the top of the outer loop resonance and the balancing point was positioned some 400 Hz below the inner loop resonant frequency (b) The same data with an expanded scale. As in Fig. 4, the circles are measurements, and the line is a fit.

In order to balance the bridge *both* at the idler and pump frequencies, the two side branches of the bridge must be fully balanced; this means that they must be balanced resistively, inductively, and capacitively. Because we were only able to balance the bridge resistively and inductively, but not capacitively, we could not balance it at more than one frequency. Therefore, we had to make a choice among three possibilities: balancing the bridge at the idler frequency, at the pump frequency, or somewhere in between.

Figure 5 shows the ratio V_{Li}/V_{gen} when the balancing point was chosen some 400 Hz below the inner loop resonant frequency. The dots are derived from measurements, and the solid line from theory. In this particular case, the balancing point was between pump and the upper sideband idler. At the balancing point there was still some resistance imbalance due to the difficulty of visual adjustment when varying the FET gate voltage pot. The shape of the balancing achieved as function of frequency was in agreement with a 4.2% residual capacitance imbalance. The worst imbalance in the vicinity of the operation region corresponded to a ratio V_{Li}/V_{gen} of 0.025. This ratio divided by 11, which was how many times the voltage across one of the capacitors (V_{cap}) was bigger than the generator voltage (V_{gen}), gave the maximum imbalance (Imb $= V_{Li}/V_{cap}$), three parts in a thousand. From this maximum imbalance, we would expect a noise leakage from the outer loop to the readout inductor smaller than three parts in a thousand at any frequency in the neighborhood of the balancing point. On the other hand, the best (minimum) measured imbalance at the balancing point, derived from other set of data, was 12 ppm.

B. Verification of the parametric damping and antidamping

The inverse mechanical decay time was measured for various conditions of pump voltage and frequency. We analyzed these results with a modified equation previously derived for a similar case, and from them we calculated the strength of the coupling this transducer was able to achieve. In agreement with the model, we observed the parametric effect of continuous and smooth variation of the loaded inverse decay time as a function of the offset between the pump frequency and the inner loop resonant frequency.

One of the characteristics of a parametric transducer is its ability to convert pump energy into energy of an electrical signal with frequency equal to the pump plus or minus the mechanical frequency, and that carries the information of the mechanical oscillator motion. This phenomenon of power transfer from one frequency to another is called the parametric effect. Although it was first discussed in 1831 by Faraday and has been studied by him and other eminent physicists such as Melde and Lord Rayleigh,[35] it was not before the middle of the 1950's that

Manley and Rowe derived the relations governing the parametric feedback.[36] Here we report experimental results that show how this parametric feedback manifests in our transducer. We vary both the pump voltage and frequency and compare the results with theory.

The Manley and Rowe power relations for a parametric system with four frequencies such as one low-frequency mechanical signal, one high-frequency electrical pump signal, and two electrical sidebands $\omega_{\text{pump}} + \omega_m$ and $\omega_{\text{pump}} - \omega_m$ are

$$-\frac{P_p^{(-)}}{\omega_p}=\frac{P_{p-m}}{\omega_p-\omega_m} \text{ and}$$

$$\frac{P_m^{(-)}}{\omega_m}=\frac{P_{p-m}}{\omega_p-\omega_m} \text{ for the } (-)\text{interaction,}^{37} \tag{1a}$$

and

$$-\frac{P_p^{(+)}}{\omega_p}=\frac{P_{p+m}}{\omega_p+\omega_m} \text{ and}$$

$$-\frac{P_m^{(+)}}{\omega_m}=\frac{P_{p+m}}{\omega_p+\omega_m} \text{ for the } (+)\text{interaction,} \tag{1b}$$

where $P_i^{(\pm)}$ is the power flowing into or out of the mode i due to the parametric interaction $(\pm)$. These equations also imply that $P_p^{(-)} - P_m^{(-)} = P_{p-m}$ and $P_p^{(+)} + P_m^{(+)} = P_{p+m}$. Therefore, the sidebands always receive a net power. In the minus interaction the minus sideband receives power only from the pump mode, and in the plus interaction it receives power from both pump and mechanical modes. Also in the minus interaction the net power received by the mechanical mode due to the parametric coupling is supplied by the pump mode. When the net power received by the plus sideband equals the power received by the minus sideband times the ratio of their frequencies $(\omega^{(+)}/\omega^{(-)})$, the mechanical mode does not receive or lose power due to the parametric interaction. We say in this case that the "loaded" Q of the mechanical mode (the effective Q when the interaction is turned on) has the same value as its "unloaded" Q. Otherwise, the loaded Q assumes different values, higher or lower than the unloaded Q depending, respectively, whether the $(-)$ or $(+)$ sideband dominates.

The parametrically coupled equations of motion for this transducer are approximately:[6]

$$\ddot{x}(t)+\frac{\omega_m}{Q_m}\dot{x}(t)+\omega_m^2 x(t)=\frac{F_m(t)}{M}+\frac{F_{\text{vib}}(t)}{M}+\frac{F_B(t)}{M}-\frac{V_{\text{cap}}(t)}{DM}q(t), \tag{2}$$

and

$$\ddot{q}(t)+\frac{\omega_{\text{ilr}}}{Q_{\text{ilr}}}\dot{q}(t)+\omega_{\text{ilr}}^2 q(t)=-\frac{V_{\text{cap}}(t)}{L_{\text{il}}}\left(\frac{x(t)}{D}\right)+\frac{V_n(t)}{L_{\text{il}}}+\frac{I_n(t)}{L_{\text{il}}}\omega_{\text{ilr}}L_i, \tag{3}$$

where x and q are the displacement and charge of the middle plate, ω_m,ω_{ilr}, Q_m, and Q_{ilr} are the angular frequencies and figures of merit for the mechanical and inner loop resonances, respectively, $F_m(t)$,$F_{\text{vib}}(t)$, and $F_B(t)$ are the forces of the mechanical signal, mechanical vibration noise, and Brownian noise (Langevin force);[38] M is the reduced mass of the system middle plate plus transducer, D is the average capacitance gap, L_{il} is the total idler inductance, L_i is the idler or readout inductance, V_n is the Johnson noise[39] of the inner loop resistance, and I_n is the amplifier current noise. The last term in Eq. (2) is the "back action" force term.

From these motion equations we can derive the expression for the loaded relaxation time of the mechanical resonator,[22] and it is equal to

$$\frac{1}{\tau_L}=\frac{1}{2}\left[\left(\frac{1}{\tau_{\text{ilr}}}+\frac{1}{\tau_m}\right)-\sqrt{\left(\frac{1}{\tau_{\text{ilr}}}-\frac{1}{\tau_m}\right)^2-f\beta\omega_m^2}\right], \tag{4}$$

where $\beta = (V_{\text{co}}/D)^2\,(\omega_{\text{ilr}}/\omega_m)\,(C/M\omega_m^2)$ is a dimensionless measure of the strength of the coupling between the mechanical and electrical modes, $V_{\text{co}} = \sqrt{2}\,V_{\text{cap}}$, $\tau_m = Q_m/\omega_m$, $\tau_{\text{ilr}} = Q_{\text{ilr}}/\omega_{\text{ilr}}$, C is the average capacitance [$C = (C_l + C_r)/2$], and f is a factor that gives the measure of the net parametric feedback. When f has a positive value, the loaded mechanical relaxation time decreases as β is increased; and when f is negative, the loaded mechanical relaxation time increases as β is increased. However, our experiment has one important distinction from that of Ref. 22. There the transducer had two pump signals, and the idler signal was localized only on the top of the inner loop resonance; here our transducer had a single pump signal and two idler signals at the pump frequency plus and minus the mechanical frequency rather than on the top of the resonance. Therefore, we had to introduce some changes in the original result.

In order to take into account the presence of the two sidebands and the fact that the pump frequency is at an arbitrary position relative to the inner loop resonant frequency, f in Eq. (4) now becomes

$$f=[\text{abs}(f_+)]^2-[\text{abs}(f_-)]^2, \tag{5}$$

where

$$f_\pm=[1/(1+j2Q_{\text{ilr}}\delta_\pm)],$$

$$\delta_\pm=(\omega_\pm-\omega_{\text{ilr}})/\omega_{\text{ilr}}, \text{ and}$$

$$\omega_\pm=\omega_p\pm\omega_m.$$

Figure 6(a) shows the inverse mechanical decay time for a pump signal of 350 mV rms across a single side of the three-plate capacitor (V_{cap}) when this pump signal varies in frequency about the inner loop resonance, and Fig. 6(b)

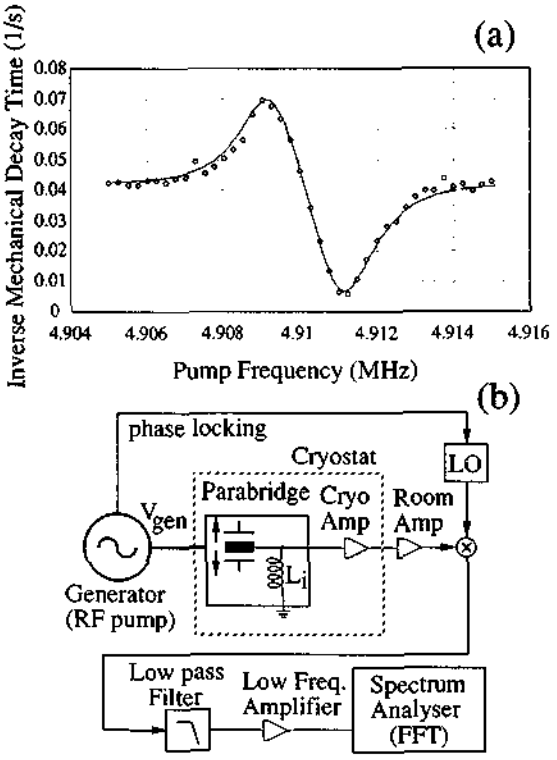

FIG. 6. Parametric damping and antidamping of the mechanical resonance, when the coupling is moderate in strength. (a) Inverse mechanical decay time plotted as function of pump frequency, and (b) equipment diagram for the measurement. The circles are measurements and the solid curve the theory [Eq. (4)]. The "loaded" decay time converges to the "unloaded" one for frequencies more than 5 kHz away from the top of the inner loop resonance, and the coincidence between the two decay times is perfect only when the pump is exactly at the inner loop resonant frequency. This case corresponds to $V_{cap} = 350$ mV rms, $Q_m = 138$ k, $Q_{ilr} = 2.2$ k, $Q_{olr} = 600$, $f_m = 929.14$ Hz, $f_{ilr} = 4.910\,100$ MHz, and $f_{olr} = 4.911\,400$ MHz. The fitting parameters were V_{cap} and f_{olr}, but V_{cap} was in the expected range given by the loop equations.

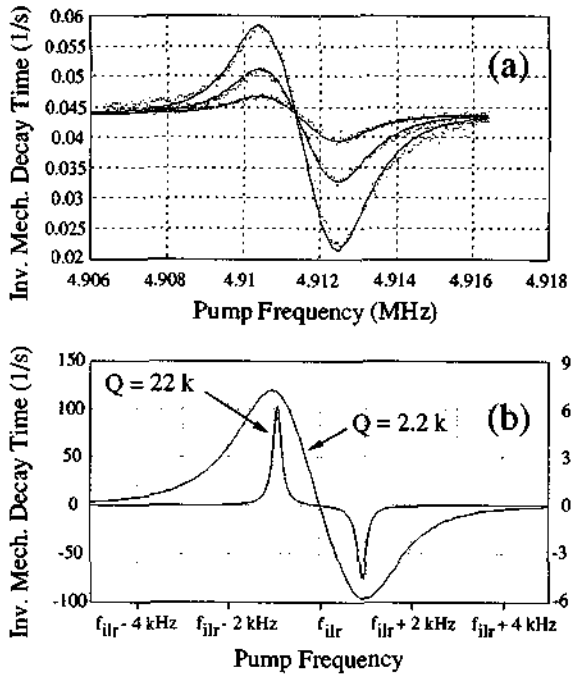

FIG. 7. (a) Inverse mechanical decay time as a function of the pump frequency for three different values of pump voltage, from highest to lowest: 291, 206, and 130 mV rms. The points are measurements and the curve is derived from Eq. (4). The case here is for: $Q_m = 133$ k, $Q_{ilr} = 2.1$ k, $Q_{olr} = 651$, $f_m = 929.14$ Hz, $f_{ilr} = 4.911\,350$ MHz, and $f_{olr} = 4.913\,100$ MHz. Again the fitting parameters were V_{cap} and f_{olr}. (b) Comparison between two predictions of Eq. (4) for different Q_{ilr}'s. One is the measured value for the present experiment, and the other a value ten times bigger. The vertical scale on the right side corresponds to the lower Q (= 2.2 k). We notice that for pump frequencies whose offset from the inner loop resonant frequency is close to 929 Hz, the parametric feedback sharply increases. The other parameters for these two cases are: $V_{cap} = 5\,V_{rms}$, $Q_m = 138$ k, $Q_{olr} = 600$, $f_m = 930$ Hz, and $f_{olr} = f_{ilr} - f_m$.

presents the equipment diagram used to measure these data. The Q_{ilr} was 2200, implying a bandwidth of about 2.3 kHz. Therefore, both sidebands had to be considered. For pump frequencies below (above) the inner loop resonance, the mechanical loaded Q assumed values smaller (bigger) than the unloaded Q. The equality of the two Q's was only possible exactly at the inner loop resonant frequency. The solid line is given by the expression above, and the dots are measured values taken with a 9000 series HP computer connected to a 3561A HP dynamic signal analyzer.

Figure 7(a) shows similar curves, now for different voltages across the capacitor. Again the dots are measurements and the solid line theory. We notice that the maximum and minimum always occur at the same frequencies above and below the inner loop resonance, which are, for the present electrical Q, about ± 1 kHz from it. Only for very high Q's they become close to ± 929 Hz. The predicted effect of higher Q's can be seen in Fig. 7(b). In the extreme case (very high Q's), there would be only two very narrow peaks, at the sum and difference frequencies. At any other pump frequency the coupling would be essentially zero.

It is interesting to observe the case when the voltage across the capacitor plates is high and we try to pump at frequencies above the inner loop resonance. The system becomes unstable and the loaded mechanical Q goes to negative values, meaning the presence of parametric oscillations. Figure 8 shows this behavior. Negative decay times were difficult to measure, and except for a few close to the inner loop resonance (small values of negative decay time), they were not measured (the oscillations were growing too fast and saturating the amplifiers). Notice the value of maximum inverse of decay time (measured when there was 8.94 V rms across the 50 μm capacitor gap): 22.2 s^{-1}, corresponding to a loaded Q of 263. This value is the result of a coupling (β) of 0.054, which is the highest measured so far for this class of transducers. Actually we could have pumped even harder by using a 3325A HP synthesizer instead of a VDS-15 synthesizer. We would have reached a $\beta \sim 1$, but at the expense of degrading the phase noise from -144 dBc/Hz presented by the VDS-15 to about 115–120 dBc/Hz.

All the measurements in Figs. 6, 7, and 8 were taken with the outer loop resonance in the region of measurement (4.906–4.944 MHz), causing a strong enhancement of pump signal across the capacitor plates. We could not

do the same at 5 MHz. Even using the VDS-15, at the same level of pumping as in Fig. 8, the voltage across the capacitor plates (V_{cap}) was only 337 mV rms ($\beta = 7.7 \times 10^{-5}$).

C. Calibration

We measured the transducer response to a calibrated force, using a capacitor plate facing the transducer body. From these measurements we calculated the total transducer gain (including amplifier chain) and the transducer sensitivity.

Calibration of ultrahigh sensitive transducers such as the ones designed for gravitational wave antennas is not an easy task.[40,41] The experimental setup must isolate the transducer from laboratory vibrations as much as possible; otherwise, a very sensitive transducer plus amplification chain may be over excited and not allow any sort of measurement. The calibration itself is another significant problem because it must be done in a manner that minimizes the degradation of the transducer performance. Fortunately, because we constructed the cryostat with high vibration isolation characteristics, and because we considerably simplified the calibration setup, we were able not only to measure a high sensitivity for this transducer, but also to observe the transducer excitation due almost exclusively to the mechanical Langevin forces from the Brownian motion.

The calibrating capacitor was composed of an aluminum disk facing an aluminum flange to which the transducer was rigidly bolted. The distance between the disk and flange was 1.45 mm corresponding to a capacitance of 28.2 pF, with systematic error of less than 5%. The transducer was set into oscillation by driving a voltage difference between aluminum disk and flange. There was a leakage of mechanical energy from the disk oscillations to the transducer, but it was very small compared to the energy transferred through the electric coupling. Taking into account the equation of motion of the vibration isolation stages between the aluminum disk and transducer, we calculated that the amplitude of oscillations on the transducer due to mechanical forces was more than four orders of magnitude smaller than the amplitude caused by the electrical force.

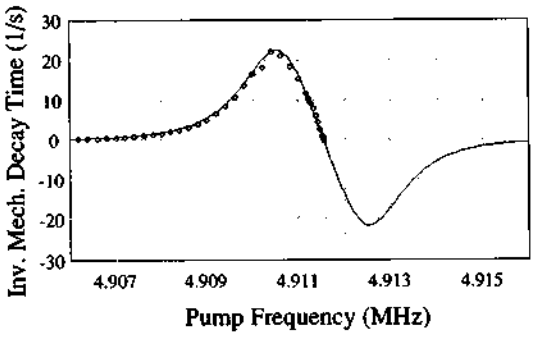

FIG. 8. Parametric damping and antidamping of the mechanical resonance for the case of highest coupling (pump voltage = 8.94 V rms). The circles are measurements, and the solid curve Eq. (4). The conditions were essentially the same as in Fig. 6; therefore, the only fitting parameter was V_{cap}, which closely agreed with the loop equations. All the unloaded Q's were the same ones supposed in Fig. 6. The only difference (besides V_{cap}) was $f_{ilr} = 4.911\,533$ MHz. The voltage across the capacitor in this set of measurements corresponds to an electromechanical coupling coefficient β of 0.054, which is the highest value ever recorded for parametric transducers made for gravitational radiation antennas.

TABLE II. The parameters of the transducer for the two noise measurements shown in Figs. 9 and 10.

rf generator	Synthesizer	Crystal oscillator
Phase noise at 929 Hz away from carrier	− 144 dBc	− 182 dBc
Generator voltage	813 mV rms	490 mV rms
Pump frequency	4 910 604 Hz	5 000 000 Hz
Inner loop resonance	4 911 533 Hz	5 000 015 Hz
Outer loop resonance	4 911 400 Hz	4 911 400 Hz
Loaded mechanical Q	263	138 k
Electromechanical coupling	0.054	2.8×10^{-5}
rms electric field strength	1.79×10^{5} V/m	4.07×10^{3} V/m
Amplification used	100	53.3×100
Transducer-amplifier total gain at FFT input	2.73×10^{9} V/m	3.46×10^{9} V/m

To avoid any problems of miscalibrations caused by a direct pickup of the calibrating signal coming from the wave generator, we chose to excite the calibrating capacitor with an electrical signal at half the mechanical resonant frequency. Thus any direct pickup reaching the spectrum analyzer (FFT) would be at half frequency. The (rms) force at the mechanical resonant frequency, acting on the transducer box due to the calibrating capacitor, was

$$F_{rms} = V_{rms}^2 C^2/(2\sqrt{2}\epsilon_0 A), \tag{6}$$

where V_{rms} was the rms capacitor voltage at half the mechanical frequency, ϵ_0 was the vacuum permittivity, A the area, and C the capacitance. This force acting continuously on the transducer box would set the transducer mechanical resonator into oscillations with a steady-state rms amplitude:

$$y_{rms} = -Q_m F_{rms}/(\omega_m^2 M_{box}), \tag{7}$$

where $\omega_m/2\pi$ is the mechanical resonant frequency, M_{box} the transducer box mass, and Q_m the unloaded mechanical figure of merit.

During calibration, the equipment configuration was similar to the one in Fig. 6(b), with the addition of a generator for calibration signals and electrical coaxial cables connecting it to the calibrating capacitor. The rms steady-state response on the FFT screen was recorded, and the equivalent voltage divided by the rms amplitude calculated by Eq. (7). This result was the total transducer-amplification gain in units of V/m. Table II shows two cases studied: (i) a very low noise synthesizer[42] (−144 dBc at single sideband 930 Hz from carrier), in its maximum pump level (813 mV_{rms}) and at the frequency of 4.910 604 MHz, in order to have the outer loop resonance strongly enhancing the voltage across the bridge capacitor; and (ii) the extremely low noise fixed frequency crystal

oscillator[43] (− 182 dBc at single sideband 930 Hz from carrier) sending a 490 mV_{rms} pump signal at 5 MHz to the bridge transformer, but with very little enhancement in the outer loop (26.5 times smaller than in the previous case)due to the impossibility of moving the outer loop resonance above 4.95 MHz.

From the results shown in Table II, we notice that if we divide the transducer-amplifier total gain at FFT input by the amplification used and by the electric field strength across the transducer capacitor, we obtain approximately the same dimensionless result: 156. This number is a measure of transducer quality and is independent of the voltage across the transducer capacitor. We named this dimensionless number "transducer quality figure," and it can be easily shown to be approximately equal to $(\sqrt{2}/4)\ Q_{ilr}\ (L_i/L_{il})$, where Q_{ilr} is the inner loop quality factor and (L_i/L_{il}) is the ratio between the readout (or idler) inductor and the total inductance in the inner loop. The factor four in the denominator comes from the product of two halves, one from the parametric mixing between the mechanical and pump signals and the other from the demodulation mixing. The precise expression of the voltage at output of the mixer is

$$V_{\text{output of mixer}}=\frac{\sqrt{2}}{4}\frac{L_i}{L_{il}}\frac{V_{cap}}{D}Q_{ilr}x_0 \times\left(\frac{\cos[\omega_m t-(\phi_- -\phi_{LO})]}{\sqrt{Q_{ilr}^2[(\omega_{ilr}/\omega_-)^2-1]^2+(\omega_{ilr}/\omega_-)^2}} +\frac{\cos[\omega_m t+(\phi_+ -\phi_{LO})]}{\sqrt{Q_{ilr}^2[(\omega_{ilr}/\omega_+)^2-1]^2+(\omega_{ilr}/\omega_+)^2}}\right), \tag{8}$$

where (V_{cap}/D) is the rms electric field strength across the capacitor plates, x_0 and ω_m are the amplitude and frequency of the mechanical oscillations, ω_+ and ω_- are the sideband frequencies, ϕ_{LO} is the rf local oscillator phase referred to the pump generator signal, and

$$\phi_\pm=-\tan^{-1}\{\omega_\pm\omega_{ilr}/[Q_{ilr}(\omega_{ilr}^2-\omega_\pm^2)]\} \tag{9}$$

are the phase shifts produced by the inner loop resonance to the sidebands. For an inner loop quality factor of 2200, the mixer output is strongly dependent on the phase difference between local oscillator and pump signal, and care should be taken to adjust this phase in order to maximize the transducer sensitivity. The optimum phase for each relative position between the pump frequency and the inner loop resonance can be found experimentally by slowly varying the phase of the local oscillator relative to the pump oscillator while continually exciting the transducer. The relative phase that obtains the maximum response on the FFT analyzer is the ideal one.

D. Noise

After calibrating the transducer we measured its response to pure noise sources and compared the results with a modified version of a noise model for parametric transducers given in Ref. 22. We had to modify this model slightly in order to cover the effect of both sidebands, to account for the fact that we had a slightly different parabridge circuit and we were using a different definition of imbalance. The final expression of the total electrical noise is the sum of:

–the voltage noise due to the pump phase noise, $S_{\phi v}(\omega_+)$ and $S_{\phi v}(\omega_-)$;

–the inner loop Johnson voltage noise, $S_{ilv}(\omega_+)$ and $S_{ilv}(\omega_-)$;

–the outer loop Johnson noise, $S_{olv}(\omega_+)$ and $S_{olv}(\omega_-)$; and

–the voltage noise due to the rf amplifier chain voltage and current noises, $S_{rfav}(\omega_+)$, $S_{rfav}(\omega_-)$, $S_{rfac}(\omega_+)$, and $S_{rfac}(\omega_-)$,

all of them calculated at the chosen reference position, the input of the first stage of the rf amplification, or in other words, across the readout inductor. Then the power spectral density of the total voltage noise (S_V), referred to this input, is the sum of the power spectral densities of all the above noises[44,45] plus the single sideband noise of the low-frequency amplification chain (S_{LF}). Because the cryogenic amplifier was an excellent current amplifier[31] ($G_c \sim 2000$) and a poor voltage amplifier ($G_v \sim 1$), the only noise in S_{LF} to be considered is the voltage noise (S_{LFav}); and in $S_{rfac}(\omega_+)$ and $S_{rfac}(\omega_-)$, we can neglect any rf current noise other than the cryoamplifier current noise. The various predicted noise contributions can be expressed as

$$S_{\phi v}(\omega_\pm)=(1/2\tau_{ilr})^2\left(\frac{|G_m(\omega_{off})|}{|J_\pm(\omega_{off})|}\right)^2 \times[(V_{cap}\mathrm{Imb}_\pm)^2 S_\phi(\omega_\pm)], \tag{10}$$

$$S_{ilv}(\omega_\pm)=(\omega_{ilr}^2/2)\left(\frac{|G_m(\omega_{off})|}{|J_\pm(\omega_{off})|}\right)^2[4k_BTL_i^2/(L_{il}\tau_{ilr})], \tag{11}$$

$$S_{olv}(\omega_\pm)=(1/2\tau_{ilr})^2\left(\frac{|G_m(\omega_{off})|}{|J_\pm(\omega_{off})|}\right)^2\mathrm{Imb}_\pm^2(4k_BTL_{ol}/\tau_{olr}), \tag{12}$$

and

$$S_{rf}(\omega_\pm)=(\omega_{ilr}^2L_i^2/2L_{il})^2\left(\frac{|G_m(\omega_{off})|}{|J_\pm(\omega_{off})|}\right)^2 S_{rfac}(\omega_\pm) + S_{rfav}(\omega_\pm), \tag{13}$$

where $G_m(\omega_{off}) = (j\omega_{off\,mec} + 1/2\tau_m)$, $\omega_{off\,mec} = \omega - \omega_m$, $G_\pm(\omega_{off}) = (j\omega_{off\,ilr} + 1/2\tau_{ilr})$, $\omega_{off\,ilr} = (\omega - \omega_m) + (\omega_+ - \omega_{ilr})$ for the upper sideband, $\omega_{off\,ilr} = (\omega - \omega_m) + (\omega_- - \omega_{ilr})$ for the lower sideband, $J_\pm(\omega_{off}) = G_m(\omega_{off})G_\pm(\omega_{off}) \pm |f_\pm|^2\beta\omega_m^2/16$, $\omega_\pm = \omega_p \pm \omega_m$, $\mathrm{Imb}_\pm$ is the ratio V_{Li}/V_{cap} (imbalance) at each sideband, L_i, L_{il}, and L_{ol} are the readout inductance, total inner loop inductance, and the total outer loop inductance, respectively, T is the temperature, and k_B is the Boltzmann constant. Note that in the expression for the Johnson noise originated in the outer loop, the resonant frequency was supposed to be close to the pump frequency and to have a

low Q, allowing us to assume a flat response in the region of interest. Evidently this term is negligible compared to the Johnson noise in the inner loop resonance for the present situation, where we have imbalances smaller than two parts in a thousand and the inverse of τ_{olr} only 3–4 times bigger than the inverse of τ_{ilr}. Note that whenever β in the expression of $J\pm$ is not null there is back action noise, which is properly taken into account by equations 10–13 above.

Another noise present in the output of the bridge is the "signal" due to the transducer resonator response to the Langevin forces, associated with the Brownian motion, and the transducer response to laboratory vibrations not filtered by the isolation system. To these noise sources we can associate two displacement spectral densities for the resonator motion S_{Lan} and S_{vib}, respectively, in m^2/Hz. The expression for S_{Lan} (Brownian) can be easily obtained by multiplying the mechanical resistance "force" spectrum density due to the thermal noise by the square of the Fourier transform of the mechanical resonator transfer function.[46,47] The square root of this result is

$$\sqrt{S_{\mathrm{Lan}}(\omega)} = \sqrt{\frac{4k_B T\omega_0/(\mu Q_0)}{(\omega_0^2-\omega^2)^2+\omega_0^2\omega^2/Q_L^2}} \qquad (14)$$

with a peak at $\omega=\omega_0$ given by

$$\sqrt{S_{\mathrm{yo}}} = 6.682\times 10^{-17} Q_L/\sqrt{Q_0}\,(\mathrm{m}/\sqrt{\mathrm{Hz}}), \qquad (15)$$

where k_B is the Boltzmann constant, $T=4.2$ K, $\mu=0.261$ kg is the transducer reduced mass, $\omega_0=\omega_m=2\pi\,929.143$, Q_L is the loaded Q, and Q_0 the unloaded one.

Now we can add the total electrical noise spectral density to this mechanical spectral density. The way to do this is to divide the total voltage spectral density (S_V) by the square of the product between the transducer quality figure and the electric field strength, or equivalently, to multiply that voltage spectral density by the square of the ratio of the total amplification gain between the bridge output and the FFT to the transducer-amplifier total gain. The square root of this result is shown in Fig. 9, compared with the total measured noise at the FFT divided by the transducer-amplifier total gain. These plotted quantities are, respectively, the theoretical and measured total equivalent displacement noise. In this case the pump frequency was almost at the inner loop resonant frequency, so the loaded mechanical Q was equal to the unloaded one, 138 000. The agreement between theory and measurement is very good, making us believe that the transducer response was due mainly to the Brownian motion of the mechanical resonator when not submitted to calibrating pulses. The vibration isolation system, built for filtering the mechanical vibrations close to the resonator frequency, was effective for this purpose.

The two extra peaks on each side of the Brownian peak are probably excess mechanical noise over the Brownian due either to vibrations that managed to pass through the isolation system or to vibrations produced there by some up conversion process, which transfers energy from very low-frequency oscillations, poorly isolated by the system, to the mechanical resonator mode.

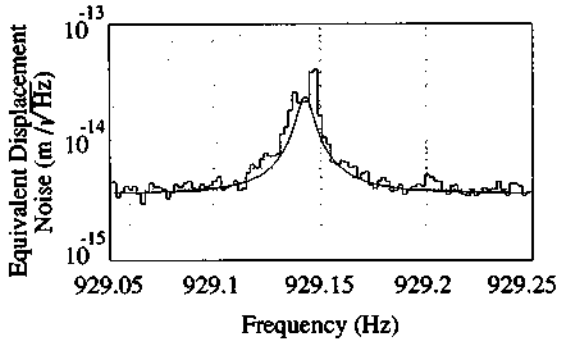

FIG. 9. Equivalent displacement noise of the transducer for a very low phase noise pump (crystal oscillator case). The stepped curve is the measured data, and the solid smooth curve is the presented noise model [Eqs. (10)–(13)] converted to $\mathrm{m}/\sqrt{\mathrm{Hz}}$. The total rf amplifier chain voltage noise at the input of the cryogenic amplifier, previously measured to be $1.45\times 10^{-9}\ \mathrm{V}/\sqrt{\mathrm{Hz}}$ for each sideband, was the dominant source of wideband noise in this case, accounting for 77% of the total wideband power spectrum density, followed by the Johnson noise generated in the inner loop resistance (22.6%). Phase noise here was completely negligible, as was the effect of the cryoamplifier current noise. The narrowband noise was dominated by the Brownian motion of the transducer resonator. The peak of the theoretical curve is due to the Brownian motion of an isolated mechanical resonator. The data are higher mainly at a side peak, that appears to be mechanical noise of unknown origin. Considering the Brownian as "signal," the transducer reached an equivalent displacement noise of $4\times 10^{-15}\ \mathrm{m}/\sqrt{\mathrm{Hz}}$, with a systematic error of less than 10%.

In Fig. 9, where the 5 MHz crystal oscillator was used as pump generator, the total rf amplifier chain voltage noise at the input of the cryogenic amplifier, previously measured to be $1.45\times 10^{-9}\ \mathrm{V}/\sqrt{\mathrm{Hz}}$ for a single sideband, was the dominant source of wideband noise in this case, accounting for 77% of the total wideband power spectrum density, followed by the Johnson noise generated in the inner loop resistance (22.6%). Phase noise here was completely negligible, as was the effect of the cryoamplifier current noise. The low-frequency amplification noise referred to the input of the cryoamplifier was responsible for most of the remaining 0.4% wideband noise. Considering the Brownian as a "signal," the transducer reached, for this crystal oscillator case, an equivalent displacement noise of $4\times 10^{-15}\ \mathrm{m}/\sqrt{\mathrm{Hz}}$, with a systematic error of less than 10%. Here two low noise rf amplifier stages[48] were used after the cryogenic amplifier.

Figure 10 shows the equivalent displacement noise using the frequency synthesizer. We observed a *dip* in the noise spectrum. Here, the Brownian noise was negligible and the phase noise was believed to be the dominant one, with 84% of the total power spectrum density. The low-frequency amplification chain voltage noise at the input of the cryogenic amplifier, previously measured to be $7.5\times 10^{-9}\ \mathrm{V}/\sqrt{\mathrm{Hz}}$ for this case, was responsible for 14.5% of the total. Because the phase noise was the most probable major source of noise in this case, and because we could not know the readout inductor to capacitor ratio of voltages for each sideband, we had to look in the model for an Imb_+ and Imb_- that could reproduce the noise floor observed and the shape of the dip. The values of these imbal-

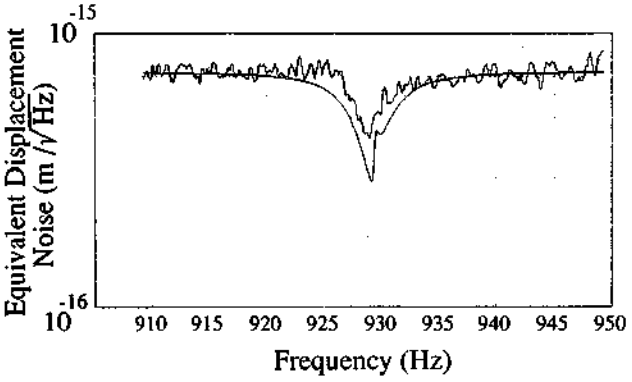

FIG. 10. Equivalent displacement noise of the transducer for the very strong coupling case (synthesizer). As in the previous figure, the smooth curve corresponds to the theoretical model, and the stepped curve to the measured data. In this case, the phase noise was the dominant, with 84% of the total power spectrum density, and the low-frequency amplification chain voltage noise was responsible for 14.5% of the total. The only fitting parameters were the imbalance factor, Imb + and Imb − . The values found for these imbalance factors were 3 and 1.5 parts in a hundred, respectively, ten times the expected values. We conjecture that the additional imbalance was caused by low-frequency oscillations of the resonator plate or other movable parts of this parabridge. There was still some remaining discrepancy between experimental data and the theoretical model, but the noise dip, close to the mechanical resonant frequency, can clearly be seen in both. The dip is a result of the parametric coupling between the electrical and the mechanical modes, and it is caused by destructive interference between the electrical noise and its "reflection" from the mechanical resonator. Due to the small loaded Q, the Brownian peak was one order of magnitude below the bottom of the dip, so the shape of the wideband noise could be fully appreciated. At the bottom of the dip the transducer achieved an equivalent displacement noise of 4×10^{-16} m/$\sqrt{\text{Hz}}$, with a systematic error of less than 10%.

ance factors that fit with data were 3 and 1.5 parts in a hundred, respectively—ten times the expected values. After this fitting,there was still some remaining discrepancy between experimental data and the theoretical model. Curiously, the agreement would be almost perfect if we had considered 1.0×10^{-8} V/$\sqrt{\text{Hz}}$ as the actual low-frequency amplification chain voltage noise.

We do not know yet why the total noise measured was about one order of magnitude higher in voltage than the total noise expected. One of the possibilities we still cannot exclude completely is an extra phase noise leakage due to additional imbalance caused by the presence of low-frequency oscillations at the resonator. These low-frequency vibrations coming from the laboratory were poorly filtered by the vibration isolation system, which was designed with the purpose of cutting mechanical vibrations higher than 500 Hz. The effect of these low-frequency vibrations(< 100 Hz) could cause a momentary bridge excess imbalance allowing, in this particular case, ten times more phase noise to leak to the readout inductor than the leakage expected from measured average imbalances.

In any case, we were able to confirm the interesting noise behavior when the frequency was close to the mechanical resonance. Thanks to the small loaded Q, the Brownian peak was one order of magnitude below the bottom of the dip, so the shape of the wideband noise could be fully appreciated. The dip is a result of the parametric coupling between the electrical and the mechanical modes. In the presence of coupling, the noise at each sideband mixes across the capacitor plates with the pump signal to produce a force acting on the mechanical resonator at its resonant frequency; on the other hand, the resonator subjected to this motion generates a "signal" at each sideband because of the presence of the pump signal across the capacitor. The expression for this "signal" reflected back can be easily derived from the initial noise injected in the circuit. The interesting fact is that this "signal" or "reflected noise" is 180° out of phase with the initial noise if the upper sideband happens to be at the electrical resonant frequency. In this case, there is a tendency of destructive interference—exactly what we observed for the synthesizer case when a high beta was used and the upper sideband was set on top of the inner loop resonance. For different relative positions of this sideband, the phase difference is no longer 180°. In particular, when the lower idler sideband is at the inner loop resonant frequency, and the regime of parametric oscillations has not been reached, the "reflected" noise is in phase with the initial electrical noise, and constructive interference occurs. This partial reduction of noise about the mechanical resonance allowed the transducer to achieve a measured equivalent displacement noise of $\sim 4 \times 10^{-16}$ m/$\sqrt{\text{Hz}}$ (error $< 10\%$), in a bandwidth of 0.7 Hz, at the bottom of the dip. This displacement noise was not smaller due to the low-frequency amplification chain voltage noise limiting the deepness of the dip.

It is an open question what effect this new observation (of a dip in the displacement noise at the mechanical resonant frequency) will have on the system sensitivity when this transducer is coupled to a gravitational wave antenna. It is a result not anticipated in any theory for gravitational wave detectors. Its effect on overall system sensitivity will require a calculation beyond the scope of this work.

IV. PROJECTIONS

With the measured equivalent displacement noise of 4×10^{-16} m/$\sqrt{\text{Hz}}$ this parametric transducer system can measure accelerations of 1.4×10^{-8} m/s^2 at 929 Hz in a bandwidth of 0.7 Hz. Evidently, much improvement is still possible. The model shows that a pump generator of phase noise as small as the crystal oscillator operating in the frequency range of our transducer's outer loop resonance would allow the transducer to reach an equivalent displacement noise of 2×10^{-17} m/$\sqrt{\text{Hz}}$ as long as 50 V_{peak} were achieved across the capacitor plates, a very easy task for a 5 V_{peak} generator. Because this amplification chain would continue to be the major source of noise, it is apparent that additional improvement would occur with the use of a lower noise amplification chain, one that would include, for example, a dc superconducting quantum interference device.

ACKNOWLEDGMENTS

We wish to thank all the other members of the LSU Experimental Relativity Group for their friendly collaboration in the various phases of this experiment. A special

thanks goes to Norbert Solomonson, who helped us with experimental and computer expertise. We also would like to acknowledge interesting discussions with Mark Bocko. This work was supported by the National Science Foundation, and one of the authors received additional support from the CNPq, the Brazilian NSF.

[1] One of us (O.D.A.) would like to suggest that a better name for gravitational wave detectors would be gravitational wave "telesensors" (in analogy to telescopes and telephones), because it correctly suggests the extension of the sense of "feeling" to far distances.
[2] J. Weber, *General Relativity and Gravitational Waves* (Interscience, New York, 1961).
[3] B. X. Xu, W. O. Hamilton, W. W. Johnson, N. D. Solomonson, and O. D. Aguiar, Phys. Rev. D **40**, 1741 (1989).
[4] E. Amaldi *et al.*, Astron. Astrophys. **216**, 325 (1989).
[5] M. Bassan, E. Cocvcia, I. Modena, G. Pizzella, P. Rapagnani, F. Ricci, paper presented at the International Workshop on GW Signal Analysis and Detection, Amalfi, Italy, 1988 (NATO ASI Conference Proceedings, to be published).
[6] W. W. Johnson and M. Bocko, Phys. Rev. Lett. **47**, 1184 (1981).
[7] V. B. Braginskii, A. B. Manukin, E. I. Popov, V. N. Rudenko, and A. A. Khorev, Sov. Phys. JETP **39**, 387 (1974).
[8] S. P. Boughn, W. M. Fairbank, M. S. McAshan, H. J. Paik, R. C. Taber, T. P. Bernat, D. G. Blair, and W. O. Hamilton, in *Gravitational Radiation and Gravitational Collapse*, edited by C. DeWitt-Morette (Reidel, Boston, MA, 1974).
[9] W. C. Oelfke and W. O. Hamilton, Acta Astron. **5**, 87 (1978).
[10] D. G. Blair, J. Mills, and R. E. Rand, IEEE Trans. Magn. **MAG-13**, 350 (1977).
[11] K. Tsubono, S. Hiramatsu, and H. Hirakawa, Jpn. J. Appl. Phys. **16**, 1641 (1977).
[12] S. P. Boughn *et al.*, in *Gravitational Radiation and Gravitational Collapse*, edited by C. DeWitt-Morette (Reidel, Boston, MA, 1974).
[13] W. C. Oelfke and W. O. Hamilton, Act Astron. **5**, 87 (1978).
[14] M. F. Bocko, L. Narici, D. H. Douglass, and W. W. Johnson, Phys. Lett. A **97**, 259 (1983).
[15] D. Blair, Phys. Lett. A **91**, 197 (1982).
[16] K. S. Thorne, C. M. Caves, V. D. Sandberg, M. Zimmermann, and R. W. Drever, in *Sources of Gravitational Radiation*, edited by L. L. Smarr (Cambridge University, Cambridge, 1979).
[17] W. C. Oelfke and W. O. Hamilton, Rev. Sci. Instrum. **54**, 410 (1983).
[18] G. Spetz, A. G. Mann, W. O. Hamilton, and W. C. Oelfke, Phys. Lett. A **104**, 335 (1984).
[19] D. G. Blair, in *Gravitational Radiation*, edited by N. Deruelle and T. Piran (North-Holland, Amsterdam, 1983).
[20] K. Tsubono, M. Ohashi, and H. Hirakawa, Jpn. J. Appl. Phys. **25**, 622 (1986).
[21] M. F. Bocko and W. W. Johnson, Phys. Rev. A **30**, 2135 (1984).
[22] M. F. Bocko, W. W. Johnson, and V. Iafolla, IEEE Trans. Magn. **25**, 1358 (1989). When Eq. (9) of this reference is corrected for a numerical error, it becomes Eq. (4) above.
[23] A set of experiments testing different plastics for mechanical Q performance made the choice of mylar the most appropriate one.
[24] W. Meyer, in *Proceedings of the Sixth International Cryogenics Engineering Conference*, edited by K. Mendelssohn (IPC, Guildford, England, 1976).
[25] W. C. Young, *Roark's Formulas for Stress and Strain*, 6th ed. (McGraw-Hill, New York, 1989).
[26] R. D. Blevins, *Formulas for Natural Frequency and Mode Shape* (Robert E. Krieger, Malabar, FL, 1986).
[27] W. E. Baker, J. Appl. Mech. **31**, 335 (1964).
[28] Lead-Zinc-Titanium piezoelectric crystal sensor.
[29] With a PWM-6 plasma needle-arc welding machine from L-TEC in a closed chamber with inert gases.,
[30] The Nb surfaces to be connected were immersed for a quarter of minute in an equal parts solution of de-ionized water, nitric acid at 70.6%, and hydrofluoric acid at 48% to break the oxide layer. Wherever it was difficult to apply the acid solution to remove the oxide layer, an oxide-free Nb blade was used to scrape it.
[31] M. G. Richards, A. R. Andrews, C. P. Lusher, and J. Schratter, Rev. Sci. Instrum. **57**, 404 (1986).
[32] D. V. Camin, G. Pessina, E. Previtali, and G. Ranucci, Cryogenics **29**, 857 (1989).
[33] C. J. Savant Jr., M. S. Roden, G. L. Carpenter, *Electronic Circuit Design, An Engineering Approach* (Benjamin-Cummings, Menlo Park, CA, 1987).
[34] R. C. Taber (private communication).
[35] W. W. Mumford, Proc. IRE **48**, 848 (1960).
[36] J. M. Manley and H. E. Rowe, Proc. IRE **44**, 904 (1956).
[37] Twenty years before Manley and Rowe's paper Hartley, another electrical engineer of Bell Labs., had already observed the validity of the second relation for the (-) interaction [R. V. L. Hartley, Bell Sys. Tech. J. **15**, 424 (1936)].
[38] P. Langevin, C. R. Acad. Sci. **146**, 530 (1908).
[39] H. Nyquist, Phys. Rev. **32**, 110 (1928).
[40] K. Kuroda, K. Tsubono, and H. Hirakawa, Jpn. J. Appl. Phys. **23**, L415 (1984).
[41] B. X. Xu, Tech. Memo. #53, Gravitational Radiation Group, Louisiana State University, 1989 (unpublished).
[42] Model VDS-15 manufactured by Sciteq Electronics, Inc., 8401 Aero Drive, San Diego, CA 92123.
[43] Model 1120S from Austron Inc., P.O. Box 14766, Austin, TX 78761, (512) 251-2313.
[44] H. W. Ott, *Noise Reduction Techniques in Electronic Systems* (Wiley, New York, 1976).
[45] M. J. Buckingham, *Noise in Electronic Devices and Systems* (Ellis Horwood Ltd., New York, 1983).
[46] F. Reif, *Fundamentals of Statistical and Thermal Physics* (McGraw-Hill, New York, 1965).
[47] D. Middleton, *An Introduction to Statistical Communication Theory* (McGraw-Hill, New York, 1960).
[48] An Anzac AM-107 amplifier of 1.4 dB noise figure and 11.1 dB gain, plus an Aercom amplifier of 23.4 dB gain and 1.81 dB measured noise figure.